Am J Physiol Regul Integr Comp Physiol 305: R748–R758, 2013.
First published July 24, 2013; doi:10.1152/ajpregu.00150.2012.

The autonomic effects of cardiopulmonary decompression sickness in swine using principal dynamic mode analysis

Yan Bai,[1] Nandakumar Selvaraj,[1] Kyle Petersen,[2,3] Richard Mahon,[2,3] William A. Cronin,[2,3] Joseph White,[4] Peter R. Brink,[5] and Ki H. Chon[1]

[1]*Department of Biomedical Engineering, Worcester Polytechnic Institute, Worcester, Massachusetts;* [2]*Naval Medical Research Center, Silver Spring, Maryland;* [3]*Uniformed Services University, Bethesda, Maryland;* [4]*Department of Family Medicine, State University of New York at Stony Brook, Stony Brook, New York; and* [5]*Department of Physiology and Biophysics, State University of New York at Stony Brook, Stony Brook, New York*

Submitted 5 April 2012; accepted in final form 18 July 2013

Bai Y, Selvaraj N, Petersen K, Mahon R, Cronin W, White J, Brink P, Chon KH. The autonomic effects of cardiopulmonary decompression sickness in swine using principal dynamic mode analysis. *Am J Physiol Regul Integr Comp Physiol* 305: R748–R758, 2013. First published July 24, 2013; doi:10.1152/ajpregu.00150.2012.—Methods to predict onset of cardiopulmonary (CP) decompression sickness (DCS) would be of great benefit to clinicians caring for stricken divers. Principal dynamic mode (PDM) analysis of the electrocardiogram has been shown to provide accurate separation of the sympathetic and parasympathetic tone dynamics. Nine swine (Sus scrofa) underwent a 15-h saturation dive at 184 kPa (60 ft. of saltwater) in a hyperbaric chamber followed by dropout decompression, whereas six swine, used as a control, underwent a 15-h saturation dive at 15 kPa (5 ft. of saltwater). Noninvasive electrocardiograms were recorded throughout the experiment and autonomic nervous system dynamics were evaluated by heart rate series analysis using power spectral density (PSD) and PDM methods. We observed a significant increase in the sympathetic and parasympathetic tones using the PDM method on average 20 min before DCS onset following a sudden induction of decompression. Parasympathetic activities remained elevated, but the sympathetic modulation was significantly reduced at onset of cutis and CP DCS signs, as reported by a trained observer. Similar nonsignificant observations occurred during PSD analysis. PDM observations contrast with previous work showing that neurological DCS resulted in a >50% reduction in both sympathetic and parasympathetic tone. Therefore, tracking dynamics of the parasympathetic tones via the PDM method may allow discrimination between CP DCS and neurological DCS, and this significant increase in parasympathetic tone has potential use as a marker for early diagnosis of CP DCS.

autonomic nervous system; sympathetic; parasympathetic; heart rate variability; cutis marmorata

DECOMPRESSION SICKNESS (DCS) results from a sudden decrease in ambient pressure and is believed to be caused by inert gas bubbles (mostly nitrogen) in tissue and blood vessels coming out of solution. When the amount of bubbles exceeds the ability of the body to diffuse them and if the bubbles grow or are present in critical locations (such as joints), DCS symptoms may appear. Although the pathohysiology of DCS is not fully known, it is likely that this excess inert gas results in intravascular and tissue-based bubbles, leading to vascular dysfunction and inflammation (31). Based on symptom severity, DCS can be divided into either type I or type II (29, 30). Type I DCS is less severe, affecting cutaneous or musculoskeletal systems ("the bends"), and includes pain as a symptom (31). Type II DCS is characterized by vestibular, cardiopulmonary, and neurological disorders, and includes symptoms such as numbness, tingling, and paralysis (31). Although the overall reported DCS incidence is low [0.035% of dives or 0.43% of divers (26a)], it appears that there is unpredictable individual susceptibility as well as potentially higher risk scenarios, especially encountered in the military.

Although there have been many preventive studies (10, 22), little effort has focused on methods to detect DCS onset. A noninvasive, unobtrusive, accurate monitoring system could provide warning of possible DCS onset to the diver or dive supervisor and facilitate data acquisition of actual DCS incidents. Changes in autonomic nervous system (ANS) dynamics may hold some promise as a predictive tool. Recent (9) and older (19, 20) studies all show clear evidence of significant alterations of the parasympathetic tone following exposure to hyperbaric environments. The dynamics of the sympathetic nervous system activity in hyperbaric environments are less clear, and results are conflicting (15, 32). Human water-immersion studies with hyperbaric pressures as high as 2,400 kPa [24 times sea-level atmospheric pressure (ATA)] have shown increased parasympathetic tone (28, 33). Measurements of increased parasympathetic activities are all based on the analysis of heart rate (HR) variability (HRV) derived from noninvasive recordings of electrocardiogram signals. Using HRV to detect DCS onset has had mixed success, largely because of exclusive reliance on power spectral density (PSD) to assess ANS dynamics. The PSD predominantly provides two frequency bands, low frequency (LF; 0.04–0.15 Hz) and high frequency (HF; 0.15–0.5 Hz). The LF band is widely accepted to reflect both sympathetic and parasympathetic nervous system activity, whereas the HF band reflects solely parasympathetic activity (14a). The ratio of LF components to HF components of the PSD is widely used as a simplified indicator of balance between the sympathetic and parasympathetic nervous systems (14a, 17). For example, a ratio of >1 indicates sympathetic dominance, and a number of <1 indicates greater presence of the parasympathetic dynamics. Although the LF-to-HF ratio is still widely used, its true efficacy as a prognostic index is questionable (11, 14a, 25) for two reasons: *1*) because the LF numerator has been erroneously assumed to reflect solely sympathetic activity despite strong parasympathetic nervous system presence in both LF and HF domains; and *2*) because PSD is a linear technique that fails to account for nonlinear properties of HR control.

To overcome the inability of PSD to separate the ANS dynamics, we recently developed and validated a novel nonlinear technique, principal dynamic mode (PDM) analysis, that accurately extracts and separates sympathetic and parasympathetic dynamics

Address for reprint requests and other correspondence: K. H. Chon, Dept. of Biomed. Eng., WPI, 100 Institute Rd., Worcester, MA 01609 (e-mail: kichon@wpi.edu).

(36). The PDM's advantages over PSD have been documented under various physiological conditions (2, 25, 34). We recently used PDM to show severe depression of both sympathetic and parasympathetic nervous activity during DCS in swine following a 613-kPa (200 fsw) bounce dive (2). Most of these swine suffered from neurological signs and spinal cord injury as assessed by H & E tissue staining. Since ECG data were recorded before and after but not during the dive, ANS dynamics for the entire dive profile were not available for assessment.

We aimed to analyze ANS dynamics using the PDM method during all phases (baseline, dive, and surface conditions) of a saturation dive to 184 kPa (60 fsw) and 15 kPa (5 fsw) for nine DCS-induced and six control swine, respectively. A saturation dive refers to tissues having absorbed the maximum partial pressure of gas at a particular depth. Continuous ECG recordings allow us to discern dynamics of the ANS during all phases of diving. Unlike the bounce dives, saturation exposures result in fewer animals with neurological and more animals with cardiopulmonary DCS. We sought to examine the similarities and differences between ANS dynamics in cardiopulmonary and spinal cord DCS.

MATERIALS AND METHODS

Experiment Protocol

The animal experiments reported here were conducted according to the principles set forth in the *Guide for the Care and Use of Laboratory Animals* (Institute of Laboratory Animal Resources, National Research Council, National Academy Press, 1996). The Institutional Animal Care and Use Committee of Naval Medical Research Center (an Association for Assessment and Accreditation of Laboratory Animal Care fully accredited facility) reviewed and approved all aspects of this protocol. All animals were maintained under the surveillance of veterinary staff.

Subjects. As part of a larger study on the use of nitroglycerin to prevent DCS, 15 neutered male Yorkshire swine (*Sus scrofa*) (we induced DCS in nine, and six were used as controls) were examined by a veterinarian upon receipt. However, note that none of the animals used for this study received nitroglycerine. Before any procedures, animals were acclimatized for 5 days in individual free-running cages with full access to environmental enrichment, water, and food (2% of body weight daily, Lab Diet Porcine Grower 5084, PMI Nutrition, Brentwood, MO). Animals received no exercise training before the experimental dive.

Predive preparation. On the day before hyperbaric exposure, animals underwent electrode placement on the body surface (three differential leads) and sterile external jugular vein catheter placement. The ECG electrodes were placed on the manubrium, on the xiphoid, and behind the left shoulder, which corresponds to mid-7th. Anesthesia induction was performed with intramuscular injection of 20 mg/kg ketamine and 2 mg/kg xylazine (Ketaject 100 mg/ml, Xyla-Ject 100 mg/ml, respectively; Phoenix Pharmaceutical, St. Joseph, MO). Anesthesia was maintained with 2–5% isoflurane (Halocarbon Products, Rover Edge, NJ) via a facemask. The external jugular vein was catheterized with a 16-gauge by 20.3-cm single lumen catheter (Braun Certofix; B. Braun Medical, Bethlehem, PA) via the modified Seldinger technique (3) and advanced until 8–10 cm extended from the skin incision site. The catheter was sutured in place with an exit site on the dorsal thorax, taped to the skin, and then brought through a vest worn by the animal; the vest also was placed over the electrodes and tied in place. Vests accommodated a 76-cm-long, 8-cm-diameter Tygon tube sheath (Cole-Parmer, Vernon Hills, IL), through which the catheter was advanced on the day of the dive. Electrocardiogram data transmitter [Data Sciences International's jacketed external telemetry (JET)] was connected to the ECG cables, and after verification of transmission the unit was removed, and the animal recovered for 1 day. Limited ambulation was assessed in the box during the observation period; full ambulation after recovery was verified before return to the holding pen, where the animal remained overnight.

On the day of the hyperbaric exposure (1 day after recovery from surgery), the subjects were placed into individual custom-designed Plexiglas boxes (26 × 54 × 38 in.) inside a steel-hulled, 450-ft.^{3} hyperbaric chamber as reported elsewhere (21). Each box allowed for an adjustable atmosphere environment in which the subjects could breathe without requiring restraints. Subjects had access to water ad libitum via a lixor fitted to the boxes. The external jugular vein catheter was connected to a sterile line, fed through a Tygon tube secured to the torso vest and a 360° swivel on the ceiling of the Plexiglas box, which allowed the animal to move freely and to make postural adjustments without twisting the line. The ECG telemetry system was reconnected, and baseline signals were acquired.

Hyperbaric exposure. For the nine swine in which we induced DCS, the chamber was pressurized with air to 184 kPa (60fsw) at a rate of 92 kPa/min (30 fsw/min) and remained at depth for 15 h. It is our experience from our previous studies, following saturation diving at 184 kPa, 80% of animals experienced symptoms of DCS (21). For the remaining six control swine, the chamber was pressurized with air to 15 kPa (5 fsw) and remained at depth for 15 h. The control depth of 15 kPa was chosen to recreate all experimental conditions yet pose an extremely low risk of DCS. Subjects were monitored via close-circuit television for any signs of distress related to middle-ear barotrauma. Chamber and box atmospheres were monitored with separate gas analyzers (Geotech Anagas Dive Analyzer, Denver, CO). The chamber O_2 concentration was maintained at 21 ± 0.02% and CO_2 at <0.05% surface equivalent. Temperature was maintained between 23.9 and 29.4°C (75–85°F) with 50 ± 5% humidity via an environmental control. After 15 h, nine DCS designated animals underwent decompression at 92 kPa/min (30 fsw/min).

Baseline ECG signals (1 day after recovery from surgery; hence data were not affected by anesthesia) were recorded starting 30 min before the hyperbaric or control exposure, continued throughout the saturation period, and continued for 120 min after surfacing or until death/euthanasia. Note that the baseline data were not available from two swine, since the ECG signals were highly corrupted with noise so that accurate R-R intervals could not be derived. All parameters related to the PSD and PDM were calculated for each 5-min segment and then averaged over 30 min. "Bottom" refers to the first half hour after animals reached 184 kPa (60 fsw) or 15.3 kPa (5 fsw); "surface" is the period after decompression but before DCS onset. It should be noted that DCS onset varied from as short as 10 min to as long as 1 h. If the surface period was >30 min, only the first half hour of the data were used. Cardiopulmonary DCS was defined as sustained (>1 min) clinical evidence of severely compromised oxygenation and hemodynamic instability, specifically any of the following: hemoglobin saturation of <80%, mean HR of >150% of baseline, and mean respiratory rate of >200% baseline. Cutis marmorata was defined as onset of a typical violaceous mottled or marbled skin pattern, as defined previously (21, 26). We used data segments for analysis following diagnosis of cutis marmorata (cutis) and cardiopulmonary (CP) DCS as determined by a trained observer. In certain cases, both cutis and CP symptoms occurred simultaneously.

ECG Analysis

ECG measurements were collected with a sampling rate of 750 Hz to allow accurate detection and identification of QRS complexes and the T-wave. After QRS complex detection, a search window using a threshold proportional to T decay rate determined the position of the T-wave terminus (18). The QRS duration, ST amplitude, T-wave amplitude, QT interval, and QT interval corrected for HR (QTc) were averaged for every 5 min of data. The QRS complexes were also used to identify heart beat locations. Once beat timing was determined, an instantaneous HR signal was created at a sampling rate of 4 Hz using a previously described technique (4). HR signals were down sampled to 2 Hz, and mean and trends were removed. Signal segments containing 600 data points, corresponding to 5 min, were used for both PDM and PSD analyses.

Analysis of HR Using Principal Dynamic Modes

The power spectrum of HRV signal contains many different frequency peaks. For example, there is a very low-frequency peak (0.01–0.04 Hz), the mid-frequency peaks (0.04–0.15 Hz), the high-frequency peaks (0.15–0.4 Hz), and frequency peak beyond 0.4 Hz, which can be considered as noise components. Among these, some frequency components are more dominant than others, as represented by the spectral magnitudes. The main problem with the PSD is that it is a linear method and cannot separate the sympathetic and parasympathetic dynamics since the latter encompasses both the low- and high-frequency range. The PDM, on the contrary, takes into account the second-order nonlinearities of HR dynamics and, among many frequencies in the HRV signal, extracts the main principal components using Eigen decomposition approach. The two principal components extracted (those with the largest eigenvector and the associated eigenvalues) represent sympathetic and parasympathetic dynamics since they have significant magnitudes at the low, and low- and high-frequency bands, respectively. Furthermore, these two principal components account for at least 80% of the entire dynamics. The feasibility of separation of the ANS dynamics via the PDM has been validated using ANS pharmacological blockades in our laboratory's previous study (34).

Thus the PDM method is based on the concept of extracting only principal dynamic components of the signal via eigen decomposition. The PDMs are calculated using Volterra-Wiener kernels based on expansion of Laguerre polynomials (23). Among all possible choices of expansion bases, some require the minimum number of basis functions to achieve a given mean-square approximation of the system output. This minimum set of basis functions is termed the principal dynamic modes of the nonlinear system. PDM specifically accounts for the inherent nonlinear dynamics of HR control, which the current PSD method is unable to do. A minimum set of basis functions is determined using the widely known principal component analysis method, where the dominant eigenvectors and eigenvalues are retained since they relate more closely to the true characteristics of the signal. Nondominant eigenvectors and eigenvalues represent noise or nonessential characteristics. Thus principal component analysis separates only the essential dynamic characteristics from a signal that is corrupted by noise. In the case of the HR signal, the dominant eigenvectors and eigenvalues should reflect the dynamics of the sympathetic and parasympathetic systems since they represent most of the spectral power of the HR. We have modified the PDM technique for use with even a single output signal of HRV data, whereas the original PDM required both input and output data. A detailed summary of the procedure has been presented in our laboratory's previous study (36), and comparison to the PSD has shown that the PDM is more accurate.

Although the PDM is a time-domain representation, we convert it to the frequency domain via the fast fourier transform (FFT). This facilitates validation of the two ANS activities, since they are usually illustrated in the frequency domain. Therefore, hereafter, we will describe the dynamic characteristics of the PDMs in the frequency domain. For this study, we used eight Laguerre functions with a memory length of 60. The calculation of PDMs, as well as determining Laguerre functions and memory lengths, have been previously described (36). The derived two main dynamics of PDMs will be referred to here as the sympathetic and the parasympathetic.

Power Spectral Density

Power spectral densities of HR data were calculated using the method of the Welch periodogram (Matlab 7.0, Natick, MA). A 128-point (frequency resolution of 0.0078 Hz) FFT with the Hanning window and 50% overlapping segments were used. We denote the LF and HF bands as 0.04–0.2 Hz and 0.2–0.6 Hz, respectively, since there was a clear separation of spectral powers between them. In addition, our choice of these spectral bands agrees with previous swine studies (16, 29). The derived sympathetic and parasympathetic dynamics of PSD will be referred to here as LF and HF, respectively.

Time-Domain Parameters

The mean HR, root-mean square of the successive difference (RMSSD), and standard deviation of normal-to-normal (SDNN) of HR intervals were calculated. We calculate the RMSSD and SDNN because they are quantitative time-domain statistical measures of HRV and have been shown to mainly reflect the modulation of the parasympathetic system and the overall ANS activity, respectively (14a). Thus these time-domain parameters are used as comparison to the PDM and PSD results.

Statistical Analysis

Data are represented as means ± SD. The one-way ANOVA was performed in SigmStat 3.0 (SPSS, Chicago, IL) to measure the difference among groups. When significant F ratios were obtained, Fisher's least significant difference (LSD) tests were used for multiple comparisons. A P value of <0.05 was considered significant.

RESULTS

The nine DCS-induced swine (72.06 ± 4.16 kg) all manifested cutis DCS. Six (66%) had concomitant cardiopulmonary (CP)

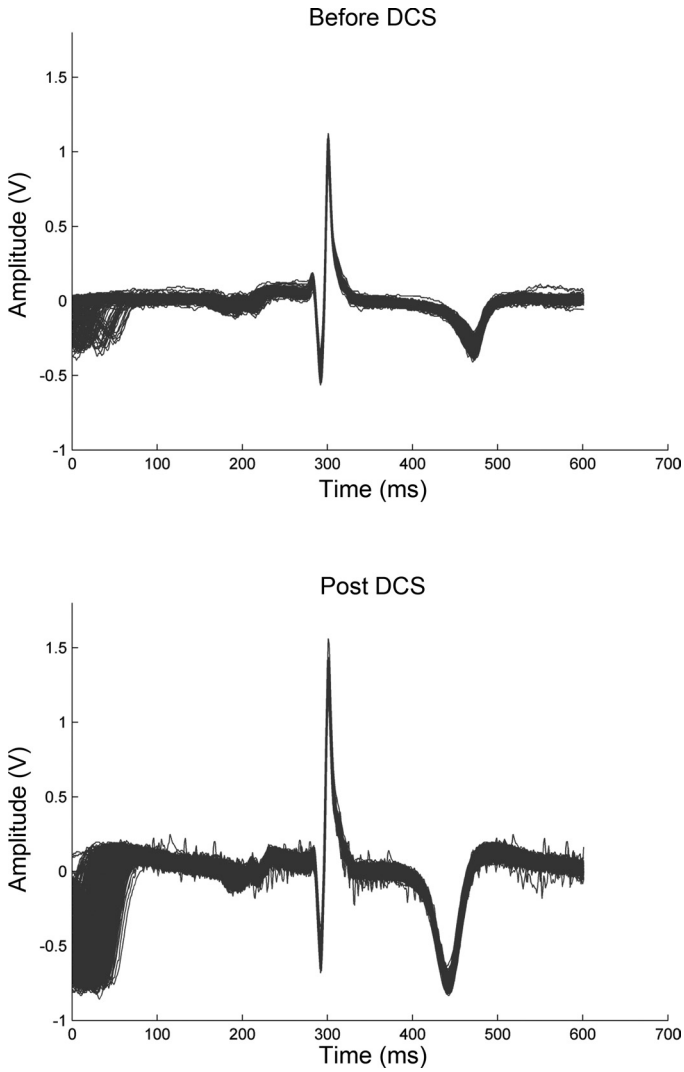

Fig. 1. The overlapped ECG of 300 beats at surface (*left*) and after decompression sickness (DCS) onset (*right*). Post-DCS T-wave became higher compared with pre-DCS condition.

Table 1. *Heart rate and ECG morphologies at different stages of the experiment for DCS-induced swine*

	Heart Rate, beats/min	QRS Duration, s	ST Elevation, V	T-Wave Amplitude, V	QT Interval, s	QTc
Baseline ($n = 7$)‡	127.33 ± 11.24	0.0638 ± 0.0013	0.00625 ± 0.0070	−0.293 ± 0.091	0.239 ± 0.013	0.346 ± 0.017
Bottom ($n = 9$)	110.34 ± 10.12*	0.0635 ± 0.0016	0.0132 ± 0.0068	−0.275 ± 0.150	0.264 ± 0.023	0.356 ± 0.020
Surface ($n = 9$)	95.29 ± 14.62*	0.0640 ± 0.0017	0.00856 ± 0.0078	−0.245 ± 0.114	0.273 ± 0.021*	0.342 ± 0.020
Cutis ($n = 9$)	109.55 ± 21.35*	0.0640 ± 0.0018	0.00215 ± 0.0152	−0.458 ± 0.193†	0.254 ± 0.024	0.338 ± 0.026
CP ($n = 6$)	120.07 ± 20.37†	0.0640 ± 0.0020	0.00952 ± 0.0367	−0.477 ± 0.259	0.247 ± 0.028	0.343 ± 0.030

All values are means ± SD. DCS, decompression sickness; QTc, QT interval corrected for heart rate. *Significant difference compared with baseline ($P < 0.05$). †Significant difference compared with surface ($P < 0.05$). ‡Note that $n = 7$ because the baseline data were significantly contaminated with noise for two swine.

signs, indicating both type I and type II DCS. No neurological signs were manifested. For the six control swine, there were no signs of either cutis or CP DCS, as determined by a trained observer.

Table 2 shows the average time of onset of cutis and CP DCS after surfacing. CP DCS onset ranged widely from 14 to 88 min; CP DCS occurred simultaneously with, or after onset of, cutis DCS.

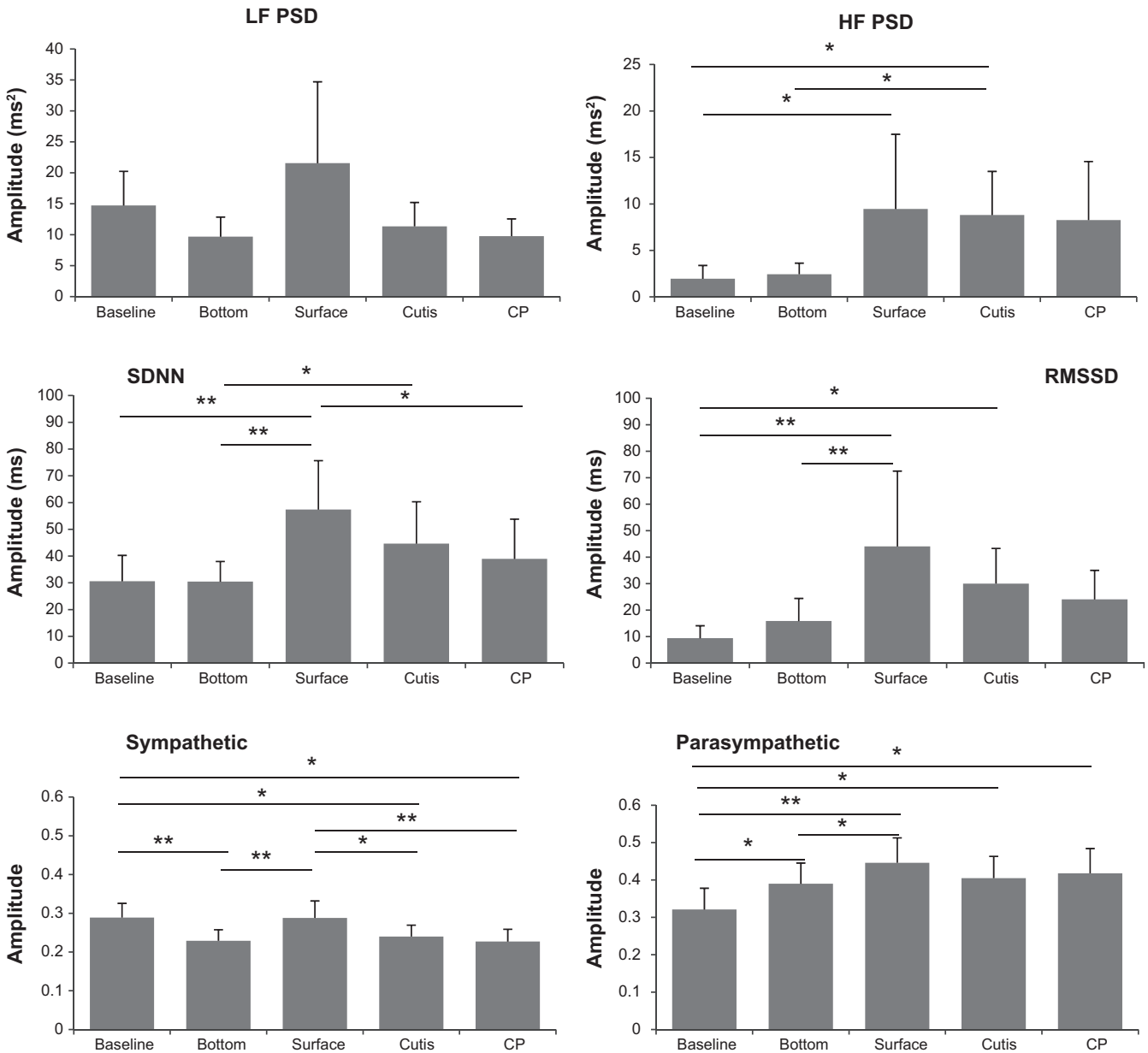

Fig. 2. Changes in heart rate variability (HRV) parameters throughout the experiment. Except for low frequency (LF) of power spectral density (PSD), all others showed significant differences: *$P < 0.05$; **$P < 0.01$.

Table 2. *Time of event onsets after surfacing for DCS-induced swine*

Event	Number of Subjects	Minutes After Surfacing
Cutis	9	37.78 ± 23.83
CP	6	41.67 ± 27.01
RMSSD	9	10.00 ± 15.00*†
HF	9	12.22 ± 15.63*†
Parasympathetic	9	9.44 ± 6.35*†

For cutis and cardiopulmonary (CP), the table shows the average onset time (±SD) of these two symptoms; $n = 9$ for all events, except CP ($n = 6$). For root-mean square of the successive difference (RMSSD), high-frequency (HF), and parasympathetic dynamics, the table lists the average time (±SD) when the postdive values of these parameters first became higher than their mean values at bottom. *Significant difference compared with cutis ($P < 0.05$). †Signficant difference compared with CP ($P < 0.05$).

ECG Morphology

One ECG cycle of 300 overlapped and aligned beats from a representative subject is shown in Fig. 1. The *left* panel shows the aligned and overlapped ECG tracings of 300 beats collected immediately after the animal reached the surface and before DCS onset. The *right* panel shows the ECG following onset of cutis DCS. T-wave amplitude was elevated and the QT interval decreased after DCS onset. The group average (Table 1) indicates that this elevation of T-wave amplitude is statistically significant. Additionally, the QT interval after surfacing significantly exceeded that of baseline. However, the QRS duration, ST amplitude, and QTc did not differ among groups (Table 1).

Hyperbaric Effect

Following the hyperbaric exposure, the sympathetic dynamics of PDM underwent a statistically significant decrease, whereas the parasympathetic dynamics underwent a statistically significant increase compared with the baseline (Fig. 2). Similarly, the LF decreased and the HF increased, but these changes were not significant (Fig. 2); the HR was significantly reduced ($P < 0.05$), however.

After Decompression

The HR nadir occurred after surfacing and before DCS onset (Table 1). The parameters SDNN, RMSSD, HF, and the parasympathetic dynamics significantly increased compared with baseline (Fig. 2). The SDNN and RMSSD values were also significantly higher than their bottom stage values.

In Table 2, three parameters representing the parasympathetic tones are shown: RMSSD, HF power, and parasympathetic tone via PDM. These three parameters can predict the onset of DCS based on the observation that the parasympathetic tones significantly increase compared with baseline and bottom stages in swine experiencing CP or cutis DCS (see also Fig. 2). We note parasympathetic tone obtained via the PDM approach has the fastest prediction of DCS onset and cutis followed by RMSSD and then HF. By using increased parasympathetic power, we can predict the onset of either cutis or CP DCS far earlier than their actual occurrence, as noted by an expert observer.

After decompression, the sympathetic dynamics were elevated ($P < 0.05$) compared with their bottom values and reached a level similar to baseline (Fig. 2). LF power followed a similar but nonsignificant trend.

Post-DCS

Following cutis or with CP DCS onset, HF and the parasympathetic dynamics were elevated compared with both baseline and bottom stages, but a significant decrease in SDNN occurred compared with the period right after surfacing (Fig. 2); there was a concomitant, nonsignificant trend of decrease in RMSSD. After cutis DCS onset, RMSSD, HF, and the parasympathetic dynamics were significantly higher than baseline, and HF also significantly exceeded its value at the bottom stage. Following CP DCS onset, the parasympathetic dynamics

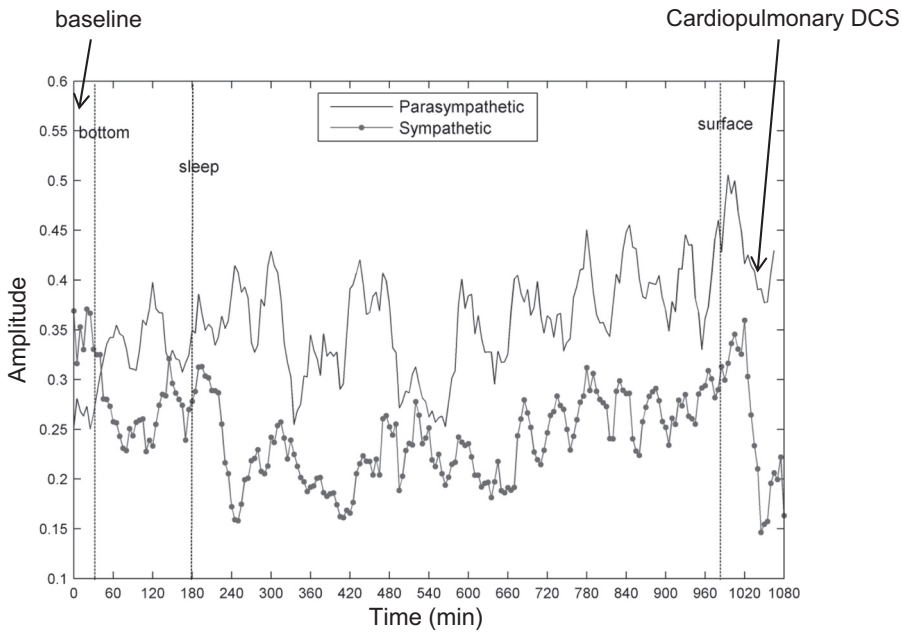

Fig. 3. The sympathetic and parasympathetic dynamics from a representative DCS-induced animal. The sympathetic (solid line with point marker) and parasympathetic (solid) dynamics were obtained through principal dynamic mode (PDM) method. The vertical broken lines indicate the experimental stages start times.

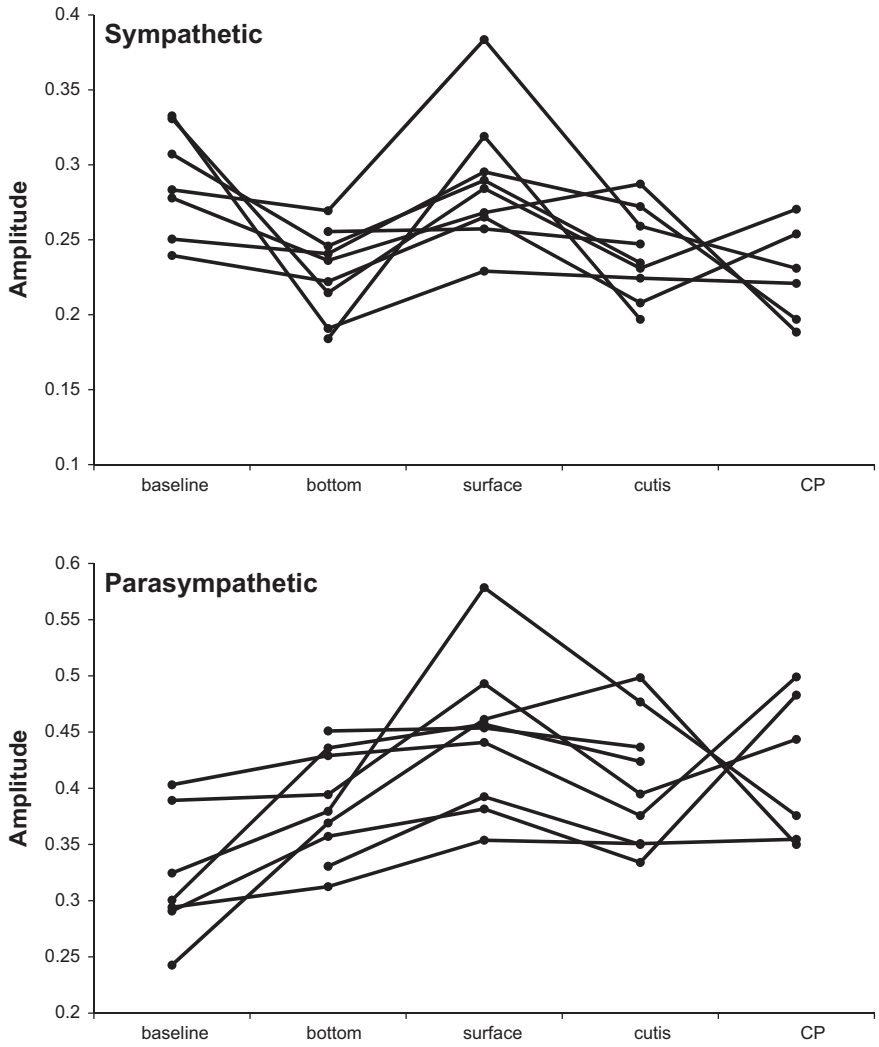

Fig. 4. The sympathetic and parasympathetic dynamics obtained by PDM for each subject at different experiments stages. Note that two subjects did not have baseline values and that three subjects did not develop cardiopulmonary (CP) DCS.

were still significantly higher than baseline, and the SDNN decreased to a level less than its value upon surfacing. The LF and the sympathetic dynamics decreased gradually from time of surface to cutis and CP DCS onset, but only the latter was significant. Furthermore, with cutis and CP DCS, the sympathetic dynamics were significantly lower compared with baseline and pre-DCS condition after decompression. As shown in Table 1, the HR gradually increased and approached its baseline value during the time from surfacing to cutis and CP DCS onset.

Figure 3 shows the sympathetic and parasympathetic dynamics of a representative subject throughout the entire hyperbaric exposure and post-surfacing observation period. It tracks the changes of the ANS dynamics during different stages of the exposure as described above. Note that, during sleep stage, the parasympathetic modulation was at a higher level than the baseline, bottom stage, and sympathetic tone.

The changes in the sympathetic and parasympathetic dynamics for each experimental stage for all swine subjects are shown in Fig. 4. Most swine demonstrated consistent trends as they transitioned from baseline to the cutis stages. In particular, eight of nine swine exhibited increased ANS dynamics as they transitioned from the bottom to the surface stage.

Control Swine (Without DCS)

HRV measures in a separate group of control swine ($n = 6$) at baseline, bottom (5 fsw) for 15 h, and back at surface pressure are provided in Table 3. Statistically significant differences between the baseline vs. surface and baseline vs. bottom were found for the

Table 3. *Heart rate variability measures obtained in control swine during dive at 5 fsw and for duration of 15 h*

	Baseline	Bottom	Surface
HR, beats/min	112.1 ± 14.1	105.9 ± 12.8	98.9 ± 10.8
SDNN, ms	18.7 ± 11.9	22.9 ± 7.3	40.0 ± 13.5
RMSSD, ms	6.4 ± 4.8	7.8 ± 4.5	15.9 ± 6.2*†
LF, beats/min^2	3.72 ± 3.94	4.76 ± 3.13	10.39 ± 6.62
HF, beats/min^2	1.01 ± 1.31	1.17 ± 0.97	3.06 ± 2.39*
LF/HF	12.88 ± 22.71	9.97 ± 9.57	7.58 ± 6.41
SNS	0.18 ± 0.08	0.18 ± 0.03	0.22 ± 0.07
PNS	0.24 ± 0.05	0.28 ± 0.06	0.34 ± 0.06
SNS/PNS	1.16 ± 0.37	1.04 ± 0.23	1.06 ± 0.17

Values are means ± SD ($n = 6$ control swine). HR, heart rate; SDNN, standard deviation of normal-to-normal; LF, low frequency; SNS, sympathetic nervous system; PNS, parasympathetic nervous system. *Significant difference compared with baseline ($P < 0.05$). †Significant difference compared with bottom ($P < 0.05$).

RMSSD; for HF, a significant difference was found between baseline and surface. All other parameters, including the PDM-derived sympathetic and parasympathetic dynamics, were not found to be different among the three conditions.

For each of the three conditions consisting of baseline, bottom, and surface, we compared control swine (without DCS induction) vs. DCS swine, and these results are shown in Figs. 5–7, respectively. For the baseline condition (Fig. 5), we observe statistically significant increases in only the LF, PNS, and SNS for the DCS swine compared with the control swine. For the bottom condition (Fig. 6), statistically significant increases in the LF, HF, PNS, and SNS were observed for the DCS swine compared with the control swine. For the surface condition (Fig. 7), statistically significant increases in the RMSSD, SNS, and PNS were observed for the DCS swine compared with the control swine.

DISCUSSION

We identified elevated parasympathetic system activity before and during the DCS development, as well as reduced sympathetic modulation post-DCS compared with the baseline and at surfacing. This is in stark contrast to our previous finding of a significant reduction (~50%) in both sympathetic and parasympathetic nervous activities following neurological DCS (2). In this study, persistent elevation of the parasympathetic dynamics during nonneurological DCS compared with the baseline is most likely the compensatory effect against inert gas bubble diffusion and protection from the deleterious effects of DCS. In addition, when animals reached the surface, their HR dropped compared with both baseline and bottom stages, but there was a trend of progressive increase in HR between reaching surface and cutis/CP DCS onset. For the control swine, we did not find differences in the PDM-derived sympathetic and parasympathetic dynamics among the three stages. However, RMSSD and HF values were elevated on the surface stage compared with the baseline conditions. The RMSSD value was also elevated for the surface stage compared with bottom conditions. We believe this could be attributed to commotions upon surface. The PDM method, however, is less affected by noise since it is designed to capture only the significant dynamics of the system and reject those dynamics that pertain to noise characteristics.

ECG Morphology

The presence of DCS signs correlated with significantly increased T-wave amplitude compared with the pre-DCS period after decompression. Although we did not directly measure potassium, a large T-wave amplitude may reflect hyperkalemia (13), which probably results from DCS-related acidosis (5, 16). The post-surface QT interval prolongation indicates bradycardia during this period since this difference was resolved with QT interval correction.

Hyperbaric Effects

Significant bradycardia was observed as the chamber pressure reached at 184 kPa (60 fsw) or the bottom stage. The

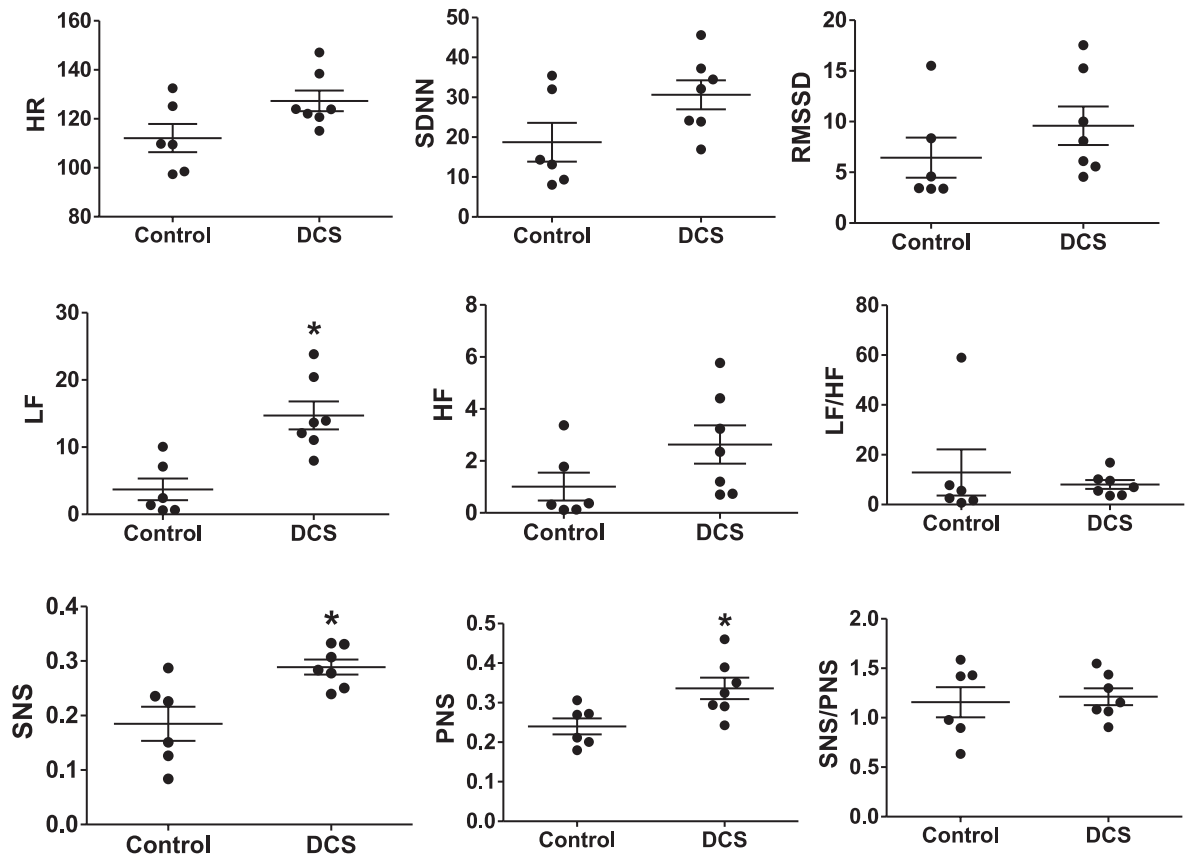

Fig. 5. Comparison of HRV parameters between control swine and DCS-induced swine at the baseline condition. Baseline condition: control ($n = 6$) vs. DCS ($n = 7$) swine. *Significant difference by Mann-Whitney test ($P < 0.05$).

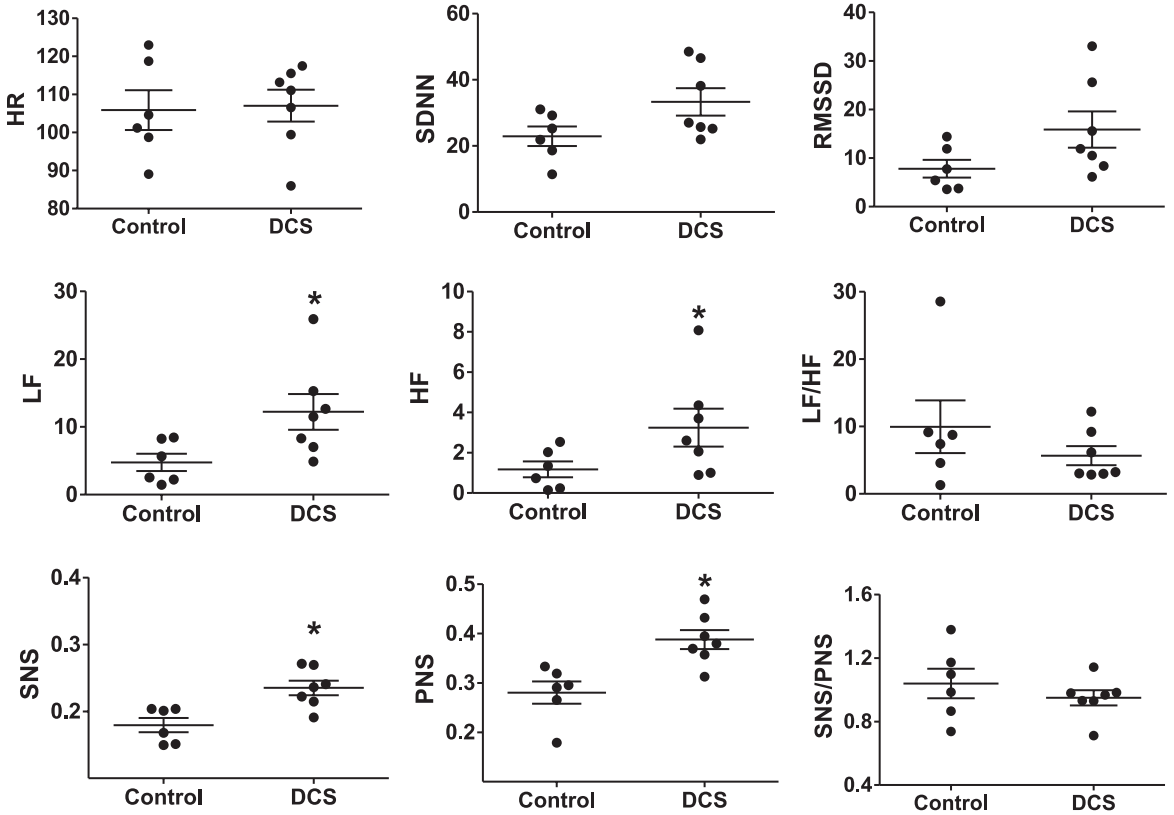

Fig. 6. Comparison of HRV parameters between control swine and DCS-induced swine at the bottom condition. Bottom condition: control ($n = 6$) vs. DCS ($n = 7$) swine. *Significant difference by Mann-Whitney test ($P < 0.05$).

mechanisms of hyperbaria-induced bradycardia are well documented (12). Decreased HR can result from the increased parasympathetic tone (14a). Hyperbaria alters the hydrostatic pressure within the systemic circulation, shunting blood from peripheral to central circulation. Increased venous return may stimulate the arterial baro- or cardiopulmonary receptors, which then alter the efferent impulses of two autonomic nervous branches, reducing HR. We observed this phenomenon. After chamber pressurization, the decrease of the sympathetic dynamics via both the PDM and the PSD, and the increased RMSSD, HF, and parasympathetic dynamics all indicate increased parasympathetic activity, consequently resulting in bradycardia.

In previous chamber studies performed at similar pressures, increased parasympathetic regulation by HF has also been noted (19, 20). However, the decreased sympathetic activity was measured via muscle sympathetic nerve activity (MSNA) (32) and not the LF. Similarly, in this study, the LF did not result in a statistically significant decrease; however, the parasympathetic did. This illustrates the greater sensitivity of the PDM compared with the PSD method. By design, the PSD, as a linear method, is unable to quantify the nonlinear properties of the ANS. More importantly, it cannot separate the sympathetic and parasympathetic components, especially in the LF band, since it contains both dynamics.

Postdive Elevation of the Parasympathetic Regulation

Post-decompression, the increase of RMSSD, HF, and the parasympathetic dynamics compared with the baseline and bottom stages indicates elevated parasympathetic modulation. However, the increase of RMSSD and HF when post-decompression (surface condition) was compared with baseline was also observed with the control swine. Note that no such increase was observed for both the parasympathetic and sympathetic derived from the PDM in the control swine; thus the PDM method is more specific than the other two methods. After DCS onset, HF and the parasympathetic dynamics did not change, whereas RMSSD showed a slight decrease. CP DCS did not significantly depress the parasympathetic tone but rather enhanced it. It should be noted that, in our laboratory's previous study, the neurological DCS significantly depressed both branches of the ANS dynamics (2). The decrease in LF and the sympathetic dynamics indicates a gradual reduction of the sympathetic regulation as the DCS development occurs. SDNN describes overall ANS activity of both sympathetic and parasympathetic branches. Right after surfacing, this parameter reached its peak value and thereafter decreased, mainly due to the reduction of the sympathetic regulation.

In a chamber study from the literature involving non-DCS decompression, the HF power for the postdive period was found to be higher than the baseline but much lower than the bottom stage (20). This suggests that, in the absence of DCS, postdive parasympathetic tone returns to normobaric environment levels but is still depressed compared with hyperbaric conditions. Thus it is reasonable to speculate that the postdive elevation of the parasympathetic modulation in this study resulted from CP DCS. In our study, the swine were saturated with inert gas at hyperbaric pressure of 184 kPa (60 fsw) for 15 h.

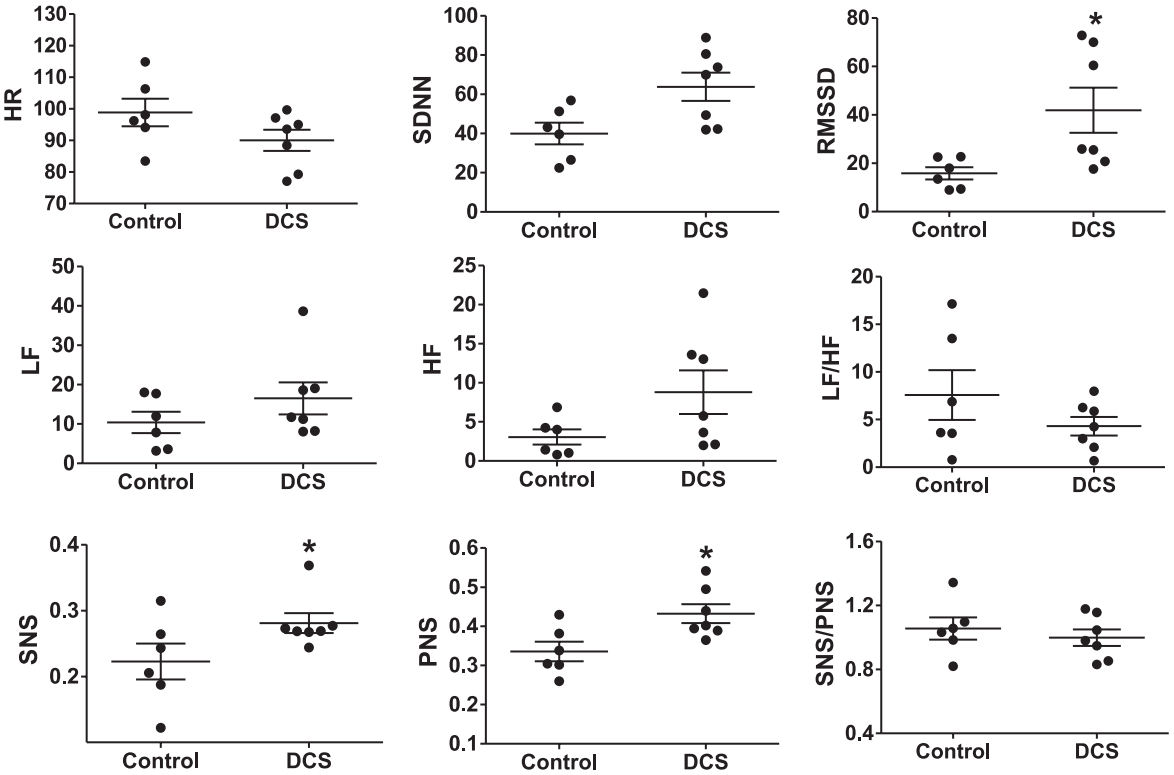

Fig. 7. Comparison of HRV parameters between control swine and DCS-induced swine at the surface condition. Surface condition: control ($n = 6$) vs. DCS ($n = 7$) swine. *Significant difference by Mann-Whitney test ($P < 0.05$).

Following rapid decompression, inert gas bubbles usually appear in veins and are diffused in the lung circulation, where they compromise the normal exchange of oxygen, causing hypoxia and increasing plasma CO_2 (5). This is followed by chemoreflex activation, enhancing amplitude and frequency modulation of respiration (30), and aiding in the diffusion of inert gases. Since the parasympathetic activity is modulated by respiration, this increase in respiratory activity could result in parasympathetic tone enhancement. Meanwhile, the chemoreflex also increases the sympathetic activity. Bubbles also cause distention of the veins, heart, and pulmonary vessels (1, 5) and may consequently stretch the cardiopulmonary receptors as if there is extra blood volume in the circulation. Consequently, this decreases the sympathetic tone and increases the parasympathetic activity (27). As bubbles accumulate, pulmonary hypertension and systemic hypotension occur (1), and these subsequently increase the sympathetic tone (24). Additionally, the increase in systemic arterial pressure reduces the parasympathetic activity through the baroreflex. It is not known whether DCS triggers hypervolemia-induced increase in the sympathetic nervous system.

After DCS onset, we observed a decrease in the sympathetic parameters of HRV compared with the surface stage. However, it seems that most of the factors discussed above should result in an increase of the sympathetic tone in DCS. Increased sympathetic activity reflects elevated HR following DCS. With pulmonary artery hypertension, a recent study found an increased muscle sympathetic nerve activity (MSNA) burst frequency and yet a reduced LF spectral component of HRV (24). This study suggested that the discordance between MSNA and the HRV LF parameter is due to the decline of the sympathetic neural modulation to HR. Furthermore, this is similar to the events in heart failure and may lead to sudden death in some patients with pulmonary hypertension (14). Considering this evidence, we speculate that in DCS there is likely an increase in the absolute amplitude of the sympathetic activity that functions to accelerate the blood circulation and bubble diffusion. However, the ability of the sympathetic system to control HR is impaired and can lead to fatal consequences in some DCS cases (2, 22).

At first glance, the post-DCS elevation of the parasympathetic modulation compared with baseline contradicts our previous study, where both branches of the ANS were significantly depressed after neurological DCS (2). In that study, both neurological DCS symptoms and spinal cord injury were observed in most of the exposed swine. Because the efferent nerves of the ANS reside in the spinal cord, the observed spinal cord injury might explain the concurrent impairment of ANS function. However, in this study, no signs of neurological DCS or spinal cord injury were observed. Since the ANS was intact, it actively regulated the cardiovascular system to protect against the detrimental effects of DCS. More importantly, the elevation of parasympathetic regulation occurred even before DCS was observed. As mentioned above, in a dive without DCS, the parasympathetic regulation immediately after surfacing should be higher than baseline but less than that found while under pressure. However, in this study, after surfacing but before DCS onset, the parasympathetic regulation was not only greater than baseline but also greater than its value during hyperbaric exposure. This implies that an abnormal elevation of the parasympathetic regulation compared with during hyperbaric exposure may portend impending DCS. Indeed, im-

mediately after surfacing but before DCS onset, an elevation of the parasympathetic regulation compared with the hyperbaric bottom stage was observed in the parasympathetic parameters we derived from the PDM. Although there was an increase in the HF and RMSSD, these cannot be considered significant since the control swine also had an increase in these values in the surface stage data compared with the baseline for the former and both baseline and bottom conditions for the latter. Since the PDM-derived parasympathetic dynamics did not increase with the control swine, we see that the PDM approach is more specific than either the PSD or RMSSD. Furthermore, although SNS and PNS for the DCS swine were greater than for the control swine for all three conditions (baseline, bottom, and surface), the further increase of the ANS dynamics seen with induction of DCS is most likely due to detrimental effects of DCS.

If we examine these parameters in each of the 5-min segments, the increased parasympathetic parameters occur immediately upon reaching surface and much earlier than DCS onset (Table 2). Thus it is possible that tracking the parasympathetic system dynamics could potentially serve as a noninvasive predictive measure for nonneurological DCS. It should be noted, however, that although we can predict the onset of cutis and CP DCS, this approach cannot distinguish between them based on the elevated parasympathetic dynamics. Distinguishing between the two may be difficult due to their simultaneous onset in six of nine swine, as reported by the observers. One additional point of note: most of the swine in this study began sleeping 30–120 min after reaching bottom; these portions of data were excluded from the computational analyses because sleep is dominated by parasympathetic activity (2). Future studies with a larger set of animals are needed to sort out these interesting questions.

Limitations

To track beat-by-beat time-varying dynamics of the ANS, time-frequency spectral analysis methods such as the wavelet have been applied (8). Our present work employing PSD, time-domain HRV parameters, and PDM methods is based on the assumption that the ANS dynamics are stationary over a 5-min data segment. However, time-varying dynamics of the ANS at each 5-min interval for the entire 15 h of data (excluding noisy portions of data and segments during sleep stages) are provided with all methods by using a sliding window approach. It should be noted that linear time-frequency methods including wavelets still have the same problem as the PSD that they cannot separate the two branches of the ANS. A time-varying PDM method is needed to obtain the separation of the dynamics of the parasympathetic and sympathetic activities on a beat-by-beat basis (35). Application of such a method is currently under progress in our laboratory.

Respiration rate, which is affected by the parasympathetic tone, was not measured during our study. Certainly, respiratory rates will vary between awake and sleep stages, and can consequently result in changes of the frequency ranges of the parasympathetic dynamics. To minimize this effect, we have excluded those portions of data that are associated with sleep when noted by a technician. Hence, we believe low breathing rates encountered at sleep overlapping with the frequency range of the sympathetic dynamics is likely to be minimal.

ACKNOWLEDGMENTS

The authors thank Melvin Routh, Catherine Jones, Madison Wilson, Wayne Koller, Pratik Patel, Jennifer Dorsey, Richard Ayres, Jeffrey Ario, William Porter, and Dale White for technical support in the design, conduct, and support of this research. The authors also thank Diana Temple for assistance in preparation of the manuscript. The opinions and assertions contained herein are those of the authors and are not to be construed as official or reflecting the views of the Department of the Navy or the U.S. Government. This work was performed by U.S. Government employees as part of their official duties; it may not be copyrighted and may be copied without restriction.

GRANTS

This work was supported by the Office of Naval Research work unit N00014-08-1-0244, N00014-12-1-0171, and Naval Sea Systems Command Work Unit Number 603713N.A0809.

DISCLOSURES

No conflicts of interest, financial or otherwise, are declared by the author(s).

AUTHOR CONTRIBUTIONS

Author contributions: Y.B., N.S., and K.H.C. analyzed data; Y.B., K.P., R.T.M., W.A.C., N.S., J.W., and K.H.C. interpreted results of experiments; Y.B. and N.S. prepared figures; Y.B. and K.H.C. drafted manuscript; Y.B., K.P., R.T.M., W.A.C., N.S., J.W., P.R.B., and K.H.C. approved final version of manuscript; K.P., R.T.M., J.W., P.R.B., and K.H.C. conception and design of research; K.P., R.T.M., and W.A.C. performed experiments; K.P., R.T.M., W.A.C., J.W., P.R.B., and K.H.C. edited and revised manuscript.

REFERENCES

1. **Atkins CE, Lehner CE, Beck KA, Dubielzig RR, Nordheim EV, Lanphier EH.** Experimental respiratory decompression sickness in sheep. *J Appl Physiol* 65: 1163–1171, 1988.
2. **Bai Y, Mahon RT, White JC, Brink PR, Chon KH.** Impairment of the autonomic nervous function during decompression sickness in swine. *J Appl Physiol* 106: 1004–1009, 2009.
3. **Bain SA, Ting J, Simeonovic CJ, Wilson JD.** Technique of venous catheterization for sequential blood sampling from the pig. *J Invest Surg* 4: 103–107, 1991.
4. **Berger RD, Akselrod S, Gordon D, Cohen RJ.** An efficient algorithm for spectral analysis of heart rate variability. *IEEE Trans Biomed Eng* 33: 900–904, 1986.
5. **Catron PW, Flynn ET Jr, Yaffe L, Bradley ME, Thomas LB, Hinman D, Survanshi S, Johnson JT, Harrington J.** Morphological and physiological responses of the lungs of dogs to acute decompression. *J Appl Physiol* 57: 467–474, 1984.
8. **Chan HL, Fang SC, Ko YL, Lin MA, Huang HH, Lin CH.** Heart rate variability characterization in daily physical activities using wavelet analysis and multilayer fuzzy activity clustering. *IEEE Trans Biomed Eng* 53: 133–139, 2006.
9. **Chouchou F, Pichot V, Garet M, Barthelemy JC, Roche F.** Dominance in cardiac parasympathetic activity during real recreational SCUBA diving. *Eur J Appl Physiol* 106: 345–352, 2009.
10. **Dainer H, Nelson J, Brass K, Montcalm-Smith E, Mahon R.** Short oxygen prebreathing and intravenous perfluorocarbon emulsion reduces morbidity and mortality in a swine saturation model of decompression sickness. *J Appl Physiol* 102: 1099–1104, 2007.
11. **Eckberg DL.** Sympathovagal balance: a critical appraisal. *Circulation* 96: 3224–3232, 1997.
12. **Flook V.** Physics and physiology in the hyperbaric environment. *Clin Phys Physiol Meas* 8: 197–230, 1987.
13. **Gurney A, Manoury B.** Two-pore potassium channels in the cardiovascular system. *Eur Biophys J* 38: 305–318, 2009.
14. **Hardegree EL, Sachdev A, Fenstad ER, Villarraga HR, Frantz RP, McGoon MD, Oh JK, Ammash NM, Connolly HM, Eidem BW, Pellikka PA, Kane GC.** Impaired left ventricular mechanics in pulmonary arterial hypertension: identification of a cohort at high risk. *Circ Heart Failure* 6: 748–755, 2013.

14a. **Heart rate variability: standards of measurement, physiological interpretation, and clinical use.** Task Force of the European Society of Cardiology and the North American Society of Pacing and Electrophysiology. *Circulation* 93: 1043–1065, 1996.

15. **Hirayanagi K, Nakabayashi K, Okonogi K, Ohiwa H.** Autonomic nervous activity and stress hormones induced by hyperbaric saturation diving. *Undersea Hyperb Med* 30: 47–55, 2003.
16. **Horner SM, Murphy CF, Coen B, Dick DJ, Harrison FG, Vespalcova Z, Lab MJ.** Contribution to heart rate variability by mechanoelectric feedback. Stretch of the sinoatrial node reduces heart rate variability. *Circulation* 94: 1762–1767, 1996.
17. **Kleiger RE, Miller JP, Bigger JT Jr, Moss AJ.** Decreased heart rate variability and its association with increased mortality after acute myocardial infarction. *Am J Cardiol* 59: 256–262, 1987.
18. **Laguna P, Thakor NV, Caminal P, Jane R, Yoon HR, Bayes de Luna A, Marti V, Guindo J.** New algorithm for QT interval analysis in 24-hour Holter ECG: performance and applications. *Med Biol Eng Comput* 28: 67–73, 1990.
19. **Lund V, Kentala E, Scheinin H, Klossner J, Sariola-Heinonen K, Jalonen J.** Hyperbaric oxygen increases parasympathetic activity in professional divers. *Acta Physiol Scand* 170: 39–44, 2000.
20. **Lund VE, Kentala E, Scheinin H, Klossner J, Helenius H, Sariola-Heinonen K, Jalonen J.** Heart rate variability in healthy volunteers during normobaric and hyperbaric hyperoxia. *Acta Physiol Scand* 167: 29–35, 1999.
21. **Mahon RT, Dainer HM, Gibellato MG, Soutiere SE.** Short oxygen prebreathe periods reduce or prevent severe decompression sickness in a 70-kg swine saturation model. *J Appl Physiol* 106: 1459–1463, 2009.
22. **Mahon RT, Dainer HM, Nelson JW.** Decompression sickness in a swine model: isobaric denitrogenation and perfluorocarbon at depth. *Aviat Space Environ Med* 77: 8–12, 2006.
23. **Marmarelis VZ.** Identification of nonlinear biological systems using Laguerre expansions of kernels. *Ann Biomed Eng* 21: 573–589, 1993.
24. **McGowan CL, Swiston JS, Notarius CF, Mak S, Morris BL, Picton PE, Granton JT, Floras JS.** Discordance between microneurographic and heart-rate spectral indices of sympathetic activity in pulmonary arterial hypertension. *Heart* 95: 754–758, 2009.
25. **Mujica-Parodi LR, Korgaonkar M, Ravindranath B, Greenberg T, Tomasi D, Wagshul M, Ardekani B, Guilfoyle D, Khan S, Zhong Y, Chon K, Malaspina D.** Limbic dysregulation is associated with lowered heart rate variability and increased trait anxiety in healthy adults. *Hum Brain Mapp* 30: 47–58, 2007.
26. **Petersen K, Soutiere SE, Tucker KE, Dainer HM, Mahon RT.** Oxygen breathing accelerates decompression from saturation at 40 msw in 70-kg swine. *Aviat Space Environ Med* 81: 639–645, 2010.
26a. *Report on Decompression Sickness, Diving Fatalities, and Project Dive Exploration*. Durham, NC: Divers Alert Network, 2008.
27. **Ricksten SE, Thoren P.** Reflex inhibition of sympathetic activity during volume load in awake normotensive and spontaneously hypertensive rats. *Acta Physiol Scand* 110: 77–82, 1980.
28. **Schipke JD, Pelzer M.** Effect of immersion, submersion, and scuba diving on heart rate variability. *Br J Sports Med* 35: 174–180, 2001.
29. **Sica AL, Ruggiero DA, Zhao N, Gootman PM.** Developmental changes in heart rate variability during exposure to prolonged hypercapnia in piglets. *Autonomic Neurosci Basic Clin* 100: 41–49, 2002.
30. **Tetzlaff K, Thorsen E.** Breathing at depth: physiologic and clinical aspects of diving while breathing compressed gas. *Clin Chest Med* 26: 355–380, 2005.
31. **Vann RD, Butler FK, Mitchell SJ, Moon RE.** Decompression illness. *Lancet* 377: 153–164, 2011.
32. **Yamauchi K, Tsutsui Y, Endo Y, Sagawa S, Yamazaki F, Shiraki K.** Sympathetic nervous and hemodynamic responses to lower body negative pressure in hyperbaria in men. *Am J Physiol Regul Integr Comp Physiol* 282: R38–R45, 2002.
33. **Yamazaki F, Shiraki K, Sagawa S, Endo Y, Torii R, Yamaguchi H, Mohri M, Lin YC.** Assessment of cardiac autonomic nervous activities during heliox exposure at 24 atm abs. *Aviat Space Environ Med* 69: 643–646, 1998.
34. **Zhong Y, Jan KM, Ju KH, Chon KH.** Quantifying cardiac sympathetic and parasympathetic nervous activities using principal dynamic modes analysis of heart rate variability. *Am J Physiol Heart Circ Physiol* 291: H1475–H1483, 2006.
35. **Zhong Y, Jan KM, Ju KH, Chon KH.** Representation of time-varying nonlinear systems with time-varying principal dynamic modes. *IEEE Trans Biomed Eng* 54: 1983–1992, 2007.
36. **Zhong Y, Wang H, Ju KH, Jan KM, Chon KH.** Nonlinear analysis of the separate contributions of autonomic nervous systems to heart rate variability using principal dynamic modes. *IEEE Trans Biomed Eng* 51: 255–262, 2004.